Journal of Power Sources 256 (2014) 66–71

Contents lists available at ScienceDirect

Journal of Power Sources

journal homepage: www.elsevier.com/locate/jpowsour

One-step hydrothermal method synthesis of core–shell $LiNi_{0.5}Mn_{1.5}O_4$ spinel cathodes for Li-ion batteries

Yuanzhuang Liu [a,b], Minghao Zhang [a], Yonggao Xia [a,*], Bao Qiu [a], Zhaoping Liu [a,*], Xing Li [b]

[a] Advanced Lithium Ions Batteries Engineering Laboratory, Ningbo Institute of Materials Technology & Engineering (NIMTE), Chinese Academy of Sciences, Ningbo, Zhejiang 315201, PR China
[b] The School of Materials Science and Chemical Engineering, Ningbo University, Zhejiang 315211, PR China

HIGHLIGHTS

- As-prepared carbonate precursor possesses concentration gradient.
- Spherical $LiNi_{0.5}Mn_{1.5}O_4$ material is core–shell structure.
- The batteries have superior rate capability and high-temperature cycle performance.
- Excellent electrochemical properties come from its unique core–shell structure.

ARTICLE INFO

Article history:
Received 10 September 2013
Received in revised form
17 December 2013
Accepted 14 January 2014
Available online 23 January 2014

Keywords:
High voltage
Core–shell structure
Concentration gradient
Rate capability
Lithium-ion battery

ABSTRACT

Spherical $LiNi_{0.5}Mn_{1.5}O_4$ material with a core–shell structure is synthesized by a urea-assisted hydrothermal method followed by heat treatment with LiOH at high temperature. After the process of hydrothermal treatment, the carbonate precursor with a concentration gradient is produced, in a single spherical particle, the content of Ni in the surface is higher than that in the center while Mn has a reversal trend. $LiNi_{0.5}Mn_{1.5}O_4$ synthesized through the hydrothermal route has a great improvement in cycling stability at elevated temperature and rate capability. The capacity retention can maintain at 95% after 30 cycles at 55 °C. Furthermore, it can deliver a discharge capacity of 118 mAh g^{-1} at a high rate of 10 C at room temperature. Such excellent electrochemical properties of $LiNi_{0.5}Mn_{1.5}O_4$ can be ascribed to its unique core–shell structure and nano-size particle.

1. Introduction

Rechargeable lithium-ion batteries (LIBs) serving as one of the most prospective power sources for personal electronic products have shown greatly potential applications in electric vehicles (EVs) and hybrid electric vehicles (HEVs) [1–4]. To achieve these usages, various cathode materials such as $LiNiO_2$, $LiMn_2O_4$ and $LiNi_{1/3}Mn_{1/3}Co_{1/3}O_2$ have been developed to be utilized in Li-ion batteries. However, due to the limitation in high-energy density or structural stability for these commercial cathode materials, other alternative candidates have been extensively explored. Among them, $LiNi_{0.5}Mn_{1.5}O_4$ has gained considerable attention by virtue of its high voltage plateau of 4.7 V, low cost and acceptable thermal stability [5–7]. Although $LiNi_{0.5}Mn_{1.5}O_4$ possessing high enough energy density can meet the requirement for vehicle applications, its high-temperature cycling performance and rate capability still confront serious challenges [8–10]. In general, capacity fading happened to $LiNi_{0.5}Mn_{1.5}O_4$ during the cycling process, especially at elevated temperature, which might be attributed to the decomposition of electrolyte and the dissolution of Mn element at high voltage [11].

To further improve its electrochemical performance, many efforts have been dedicated to elements doping and preparation of nanoparticles. Cations or anions doping are expected as effective ways to improve the performance of $LiNi_{0.5}Mn_{1.5}O_4$. Zhong et al. studied the influence of introducing Fe, Co, Cr ions into $LiNi_{0.5}Mn_{1.5}O_4$ spinel structure, showing better electrochemical performance than un-doped sample at elevated temperature [12]. Unfortunately, the modifications through doping occasionally give rise to increment in the polarization and also have a limited capacity for restraining Mn dissolution. On the other hand, in spite of nanostructured $LiNi_{0.5}Mn_{1.5}O_4$ with shortened transport distance

* Corresponding authors. Tel./fax: +86 574 8668 5096.
E-mail addresses: xiayg@nimte.ac.cn (Y. Xia), liuzp@nimte.ac.cn (Z. Liu).

0378-7753/$ – see front matter © 2014 Elsevier B.V. All rights reserved.
http://dx.doi.org/10.1016/j.jpowsour.2014.01.059

for Li and large specific surface area has advantages in enhancing rate capability, it also increases the risk of surface side reactions. Besides, its low tap density renders a lower volumetric energy density which is more detrimental [13–15].

In addition, surface coating is considered as another approach to improve electrochemical property of cathode materials [16–19]. Nevertheless, various oxides or phosphates coated on the surface of $LiNi_{0.5}Mn_{1.5}O_4$ weaken its rate performance. Thus, based on the surface modification, the core–shell structure has gradually make appeal to researchers. The core–shell structures usually possess unique physical and chemical characteristics to improve the performance, which stems from restricting the formation of a solid electrolyte interphase (SEI) and volume expansion. More recently, Jo et al. reported a nanoparticle-nanorod core–shell $LiNi_{0.5}Mn_{1.5}O_4$ delivering reversible capacity of 100 mAh g^{-1} at 7 C with no capacity fading [20].

In this paper, we firstly introduced a urea-assisted hydrothermal method followed by calcination with LiOH to synthesize homogeneously spherical $LiNi_{0.5}Mn_{1.5}O_4$ with a core–shell structure. As shown in Fig. 1, by using this strategy, we can easily prepare carbonate precursor with a concentration gradient and the resulting $LiNi_{0.5}Mn_{1.5}O_4$ maintains the concentration gradient in some extent. Furthermore, as-obtained core–shell $LiNi_{0.5}Mn_{1.5}O_4$ shows better cycling performance and rate capability.

2. Experimental

2.1. Synthesis

In a typical synthesis of spherical $LiNi_{0.5}Mn_{1.5}O_4$ powders, 12.5 mmol of $NiSO_4 \cdot 6H_2O$ (Sinopharm Chemical Reagent Co., Ltd), 37.5 mmol of $MnSO_4 \cdot H_2O$ (Sinopharm Chemical Reagent Co., Ltd) and 0.1 mol of urea (Sinopharm Chemical Reagent Co., Ltd) were dissolved in 250 ml deionized water, and then the solution was transferred to 100 ml Teflon-lined autoclave. The sealed reactor was kept at 180 °C for 12 h, after that it cooled down to the room temperature naturally. During this process, there was no escape of water.

The reactions involved in the hydrothermal treatment were complicated, including the decomposition of urea into ammonia and carbon dioxide and the formation of carbonate. Besides, ammonium sulfate produced by hydrothermal reaction decomposed reversibly while heating the reactor according to Equation (1) [21]. The whole reaction equation can be described as Equation (2).

$$(NH_4)_2SO_4 \leftrightharpoons NH_4HSO_4 + NH_3 \quad (1)$$

$$NiSO_4 + 3MnSO_4 + 4CO(NH_2)_2 + 8H_2O \rightarrow 4(Ni_{0.25}Mn_{0.75})CO_3 + 4NH_4HSO_4 + 4NH_3 \quad (2)$$

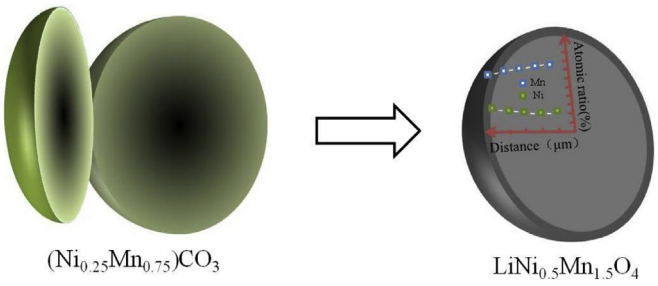

Fig. 1. Schematic illustration of the formation of the core–shell spinel structure with a concentration gradient.

The as-obtained carbonate powder was washed several times with deionized water to remove impurities. Then, the carbonate precursor was pre-sintered at 500 °C for 3 h for converting into oxides. Thereafter, the oxide powders were mixed with a stoichiometric amount of $LiOH \cdot H_2O$ (Sinopharm Chemical Reagent Co., Ltd) and calcined at 850 °C for 12 h in air to obtain the final product of $LiNi_{0.5}Mn_{1.5}O_4$.

2.2. Characterizations

Fourier transform infrared spectroscopy (FT-IR) analysis was performed on a pellet made of active materials and KBr powder by using a spectrometer (Nicolet, 6700 series, USA) to determine the composition of samples. X-ray powder diffraction (XRD) data were collected using an AXS D8 Advance diffractometer with Cu Kα radiation. The morphology and particle size were observed by scanning electron microscope (SEM, FEI Quanta FEG 250). The chemical element compositions in the product were examined quantitatively with inductive coupled plasma (ICP) with an emission spectrometer (Optima 2100 DV, Perkin–Elmer).

2.3. Electrochemical measurements

Electrochemical charge/discharge measurements were performed by CR2032-type coin cells with metallic lithium as anode electrode. The cathodes were prepared with a composition of 80 wt. % active materials, 10 wt. % acetylene black, and 10 wt. % polyvinylidene fluoride (PVDF). A cathode area specific loading was maintained at about 3 mg cm^{-2}. The electrolyte was consisted of 1 M $LiPF_6$ solution in a mixture of ethylene carbonate (EC)/dimethyl carbonate (DMC) (1:1 by volume), containing 15 ppm of water. A Celgard 2502 membrane was performed as the separator. The cells were fabricated in an argon-filled glove box in which the water content was controlled below 0.1 ppm.

Galvanostatic charge/discharge cycling curves were measured between 3.0 and 5.0 V in different current density with an LAND-CT2001A battery test system (1C-rate is equal to 147 mA g^{-1}). Cyclic voltammetry (CV) curve was inspected between 3.5 and 5.0 V by PGSTAT302 Autolab under the scan rate of 0.2 mV s^{-1}.

3. Results and discussion

To confirming the component of hydrothermal product, FT-IR is employed and the result is shown in Fig. 2. It is obvious that there are three strong adoption peaks at 1440 cm^{-1}, 862 cm^{-1}, 728 cm^{-1}, corresponding to the IR-active modes of CO_3^{2-} [22]. While the other broad peak at around 3438 cm^{-1} is ascribed to the stretching

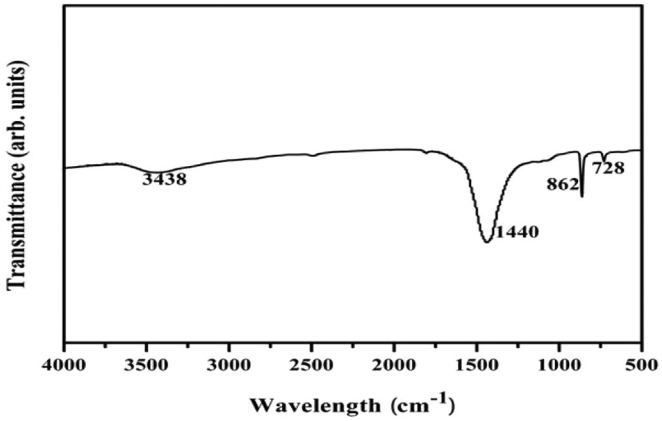

Fig. 2. FT-IR pattern of the carbonate precursor.

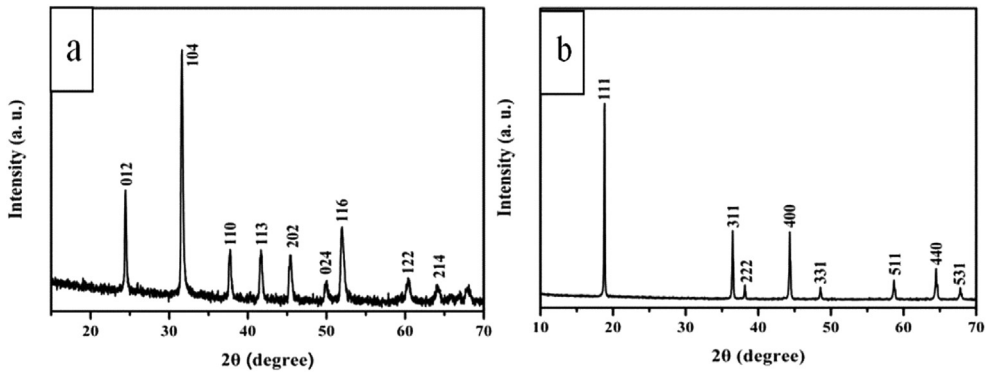

Fig. 3. XRD patterns of (a) $(Ni_{0.25}Mn_{0.75})CO_3$, (b) $LiNi_{0.5}Mn_{1.5}O_4$.

vibration of water molecules, absorption in moist air [23]. This confirms that a carbonate precursor has been obtained after hydrothermal treatment.

Fig. 3a shows the XRD pattern of the carbonate precursor and all the peaks can be indexed as a typical hexagonal structure with a space group of R-3c, which corresponds to $MnCO_3$ (JCPDS NO. 44-1472) or $NiCO_3$ (JCPDS NO. 12-0771). This is consistent with the conclusion of IR. Moreover, the molar proportion of Ni and Mn is about 1:3 detected by ICP analysis. Consequently, the molecular formula of carbonate can be expressed as $(Ni_{0.25}Mn_{0.75})CO_3$. Fig. 3b is the XRD pattern of $LiNi_{0.5}Mn_{1.5}O_4$, sharp diffraction peaks could be observed, indicating a high crystallinity of the sample. All peaks can be well indexed to the cubic spinel structure without any impurity phase.

Fig. 4a and b shows the morphology and size of $(Ni_{0.25}Mn_{0.75})CO_3$ at different magnifications by SEM. It can be seen that they are uniform spherical particles with a diameter around 25 μm (Fig. 4a). When the image of particle is enlarged as shown in Fig. 4b, the surface of the as-prepared $(Ni_{0.25}Mn_{0.75})CO_3$ is not smooth but is composed of primary nanoparticles.

Further investigations are carried out to characterize the $(Ni_{0.25}Mn_{0.75})CO_3$ sample. Fig. 5 illustrates the elemental distribution of Ni and Mn within a single particle, which shows the particle with a concentration gradient. The energy dispersive X-ray spectroscopic (EDXS) analysis of the semi-sphere is shown in Fig. 5b. It is clearly revealed that Mn element in the center part appears a little less compared to that in outer, while the Ni element presents a reverse tendency. It is worth pointing out that the mole ratio of Ni/Mn is close to the initial proportion at the core of the particle, however, at the surface, the content of Ni is significantly higher than that of Mn. On the basis of this result, we speculate that sufficient carbon source derived from urea hydrolysis at the initial stage ensures homogeneous precipitation of Ni and Mn. With the decrease of the amount of urea, the more insoluble Mn takes preference over Ni to deposit on the outside of the core. Consequently, the relatively abundant Ni precipitates at the surface in the later stage.

Fig. 5c and d presents the elemental mapping of Ni and Mn for the carbonate precursor. It is clear that these two elements homogenously distribute from the point of dense accumulation of Ni and Mn, indicating that $MnCO_3$ and $NiCO_3$ have occurred in well defined co-precipitation instead of deposition in different particles. Moreover, EDXS tests confirm that the atomic ratios of Ni and Mn are close to the primary stoichiometric proportion.

Fig. 6 shows the SEM images of $LiNi_{0.5}Mn_{1.5}O_4$ synthesized by calcining precursor with LiOH, a higher scale image embedded in the inset. From Fig. 6a, we can see that the $LiNi_{0.5}Mn_{1.5}O_4$ particles preserve the spherical morphology and the average particle size is approximately 20 μm in diameter. The size of the as-prepared $LiNi_{0.5}Mn_{1.5}O_4$ is slightly smaller than its carbonate precursor, which was also observed in the process of synthesizing spinel $Mn_{1.5}Co_{1.5}O_4$ [24]. However, the dimension of the primary particles has somewhat grown compared to that in the precursor. That is because lithiation reaction happens and crystal growth occurs at high temperature. Furthermore, the surface of the particle becomes smoother and highly porous, during the heat treatment,

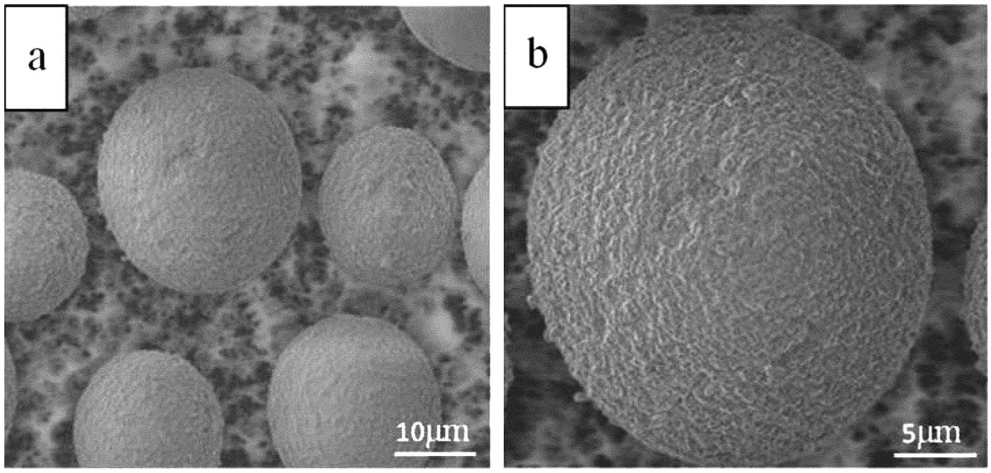

Fig. 4. (a) Low-magnification SEM image of $(Ni_{0.25}Mn_{0.75})CO_3$; (b) higher-magnification SEM image of a representative $(Ni_{0.25}Mn_{0.75})CO_3$ particle.

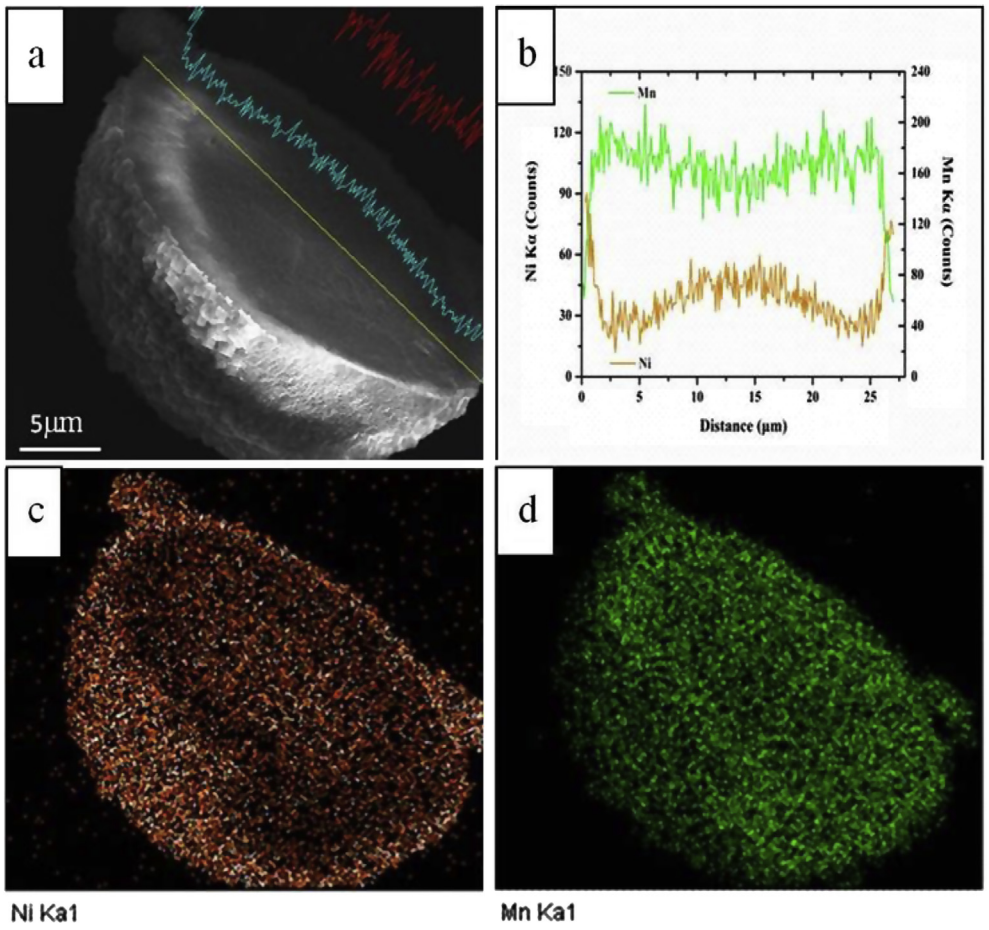

Fig. 5. Elemental analysis for a single particle : (a) cross-sectional SEM image of the $(Ni_{0.25}Mn_{0.75})CO_3$; (b) line scan of the atomic ratio of Ni and Mn as a function of the distance; SEM mapping photograph of Ni and Mn for (c) and (d) respectively.

due to the meltdown of the well-defined subunits and the emission of carbon dioxide. This porous structure can provide a larger specific surface area, enlarging the interface between electrode and electrolyte, which is in favor of Li^+ fast diffusion [25]. Interior configuration can be easily observed from a typical broken hemisphere (Fig. 6b). Owing to the existence of concentration gradient, in the course of high-temperature lithiation, heterogeneous heating treatment from surface to center and transition metals (Ni and Mn) diffusion result in the formation of a core–shell structure [24]. And it can be observed that the thickness of the shell is about 1.1 μm. Such a core–shell structure is supposed to effectively suppress large volume swing during the charge–discharge cycles and perform a better electrochemical performance [26].

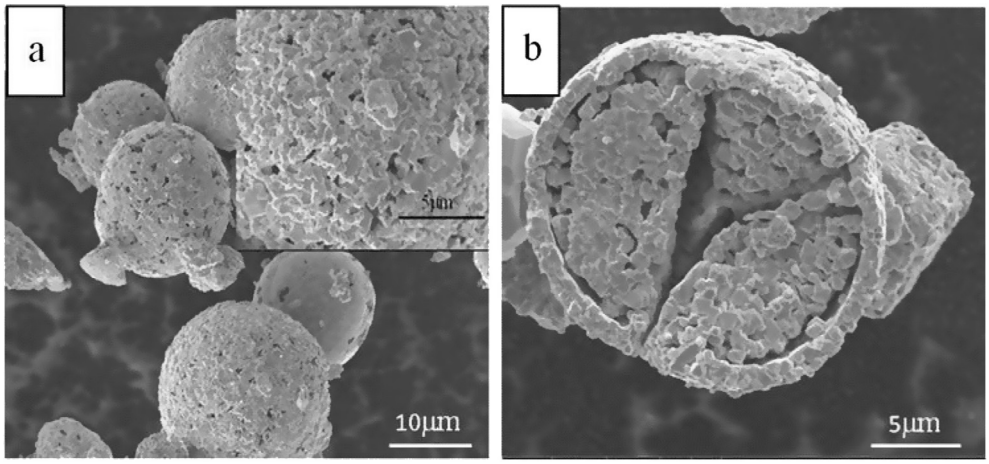

Fig. 6. SEM images of the: (a) $LiNi_{0.5}Mn_{1.5}O_4$ cathode at low magnification, the inset shows a magnified particle and (b) cross-sectional image of a single particle.

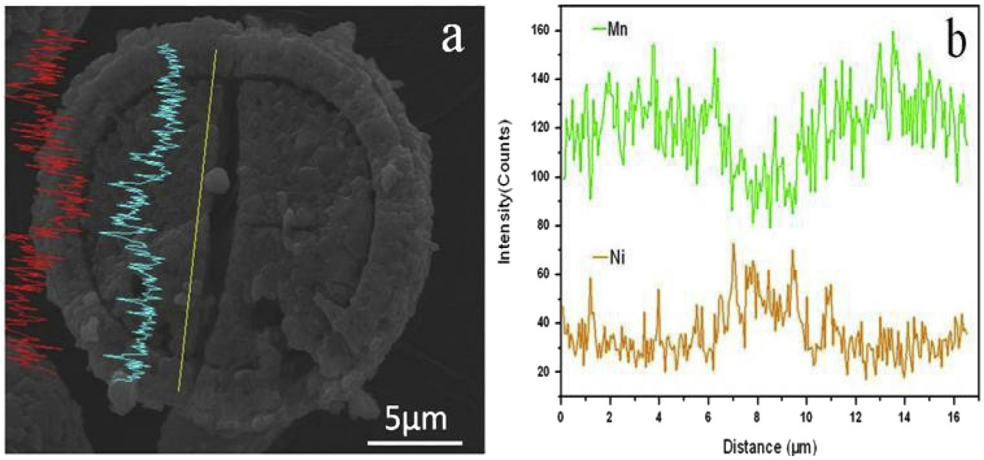

Fig. 7. (a) SEM image of cross-section of the core–shell $LiNi_{0.5}Mn_{1.5}O_4$ particles (b) line scan of the atomic ratio of Ni and Mn as a function of the distance.

In order to investigate the changes in atomic ratio of transition metals from center to surface, SEM and EDXS data of $LiNi_{0.5}Mn_{1.5}O_4$ are collected and demonstrated in Fig. 7. As exhibited in Fig. 7b, the distribution trends of Ni and Mn are still maintained compared to carbonate precursor, while the ratio of Ni/Mn in $LiNi_{0.5}Mn_{1.5}O_4$ has deviated. This result may be attributed to the influence of elements diffusion at the calcination process. Therefore, this $LiNi_{0.5}Mn_{1.5}O_4$ microsphere not only has core–shell structure but also possess concentration gradient.

Fig. 8a shows the first-cycle charge–discharge curves of this novel $LiNi_{0.5}Mn_{1.5}O_4$ cathode, in which one typically dominant discharge voltage plateau around 4.7 V emerges due to the two pairs of redox couple Ni^{2+}/Ni^{3+}, Ni^{3+}/Ni^{4+}. But, a minor plateau of 4.0 V can also be seen owing to Mn^{3+}/Mn^{4+} couple. In order to characterize redox reaction of the $LiNi_{0.5}Mn_{1.5}O_4$, cyclic voltammetry (CV) test was carried out in the voltage range from 3.0 V to 5.0 V (Fig. 8b). The CV result agrees well with the first charge–discharge curves and the primary doublet redox peaks around 4.6–4.9 V stem from the transformation of Ni^{2+}/Ni^{3+} and Ni^{3+}/Ni^{4+} [12]. Nevertheless, the slight redox peaks appearing at the range of 3.9–4.2 V are associated with the Mn^{3+}/Mn^{4+} redox couple. It means that there exists somewhat oxygen deficiency in the obtained $LiNi_{0.5}Mn_{1.5}O_4$, which arises from the loss of oxygen during the process of high sintering temperature and long reaction time [27,28]. After 50 charge–discharge cycles, the obtained CV curve almost coincides with the initial one except for the oxidation peak related to Mn^{3+}/Mn^{4+}decreases, which illustrates the $LiNi_{0.5}Mn_{1.5}O_4$ with excellent reversibility and stable structure.

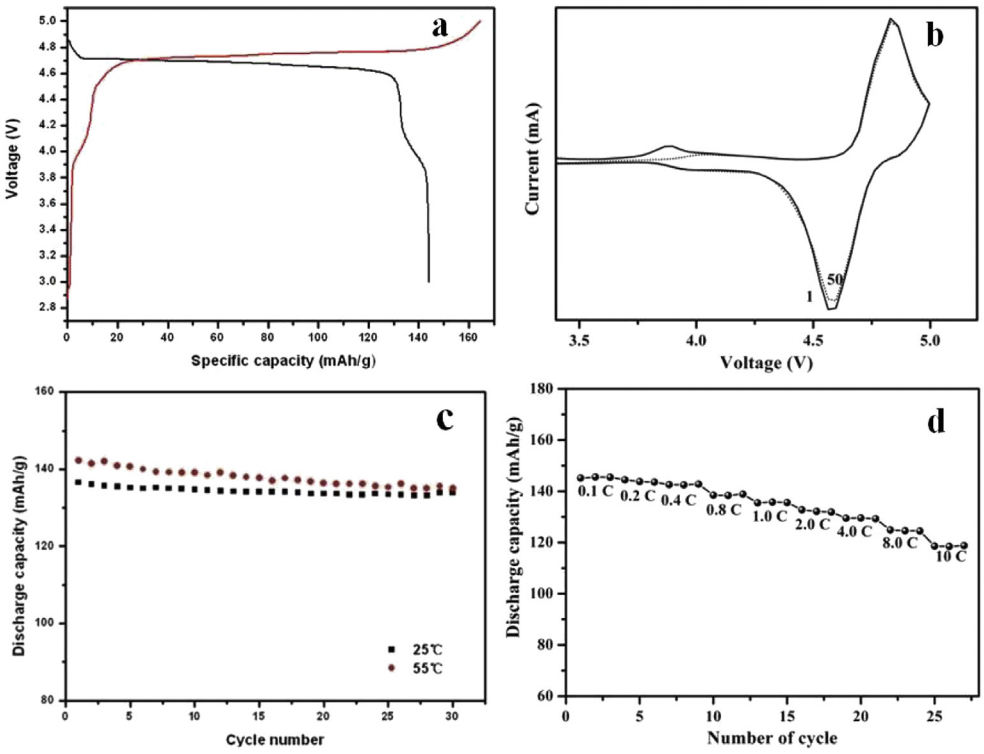

Fig. 8. (a) Initial discharge curve of $LiNi_{0.5}Mn_{1.5}O_4$ at a rate of 0.1 C and room temperature; (b) cyclic voltammetry profile between 3.0 and 5.0 V at a scanning rate of 0.2 mV s^{-1}; (c) cycling performances at 25 °C and 55 °C by applying constant current of 1 C; (d) discharge capacities of $LiNi_{0.5}Mn_{1.5}O_4$ at various C rates.

The cycling properties of the sample are examined at 25 °C and 55 °C, charged at the rate of 1 C for 30 times (Fig. 8c). The $LiNi_{0.5}Mn_{1.5}O_4$ cathode exhibits superior cyclability at 25 °C, for example, the capacity retention ratio is close to 98% after 30 cycles. Besides, the cycling performance is good even at elevated temperature and the discharge capacity can maintain at about 135 mAh g^{-1} after 30 cycles. The discharge capacities at various rates as a function of cycle number for the $LiNi_{0.5}Mn_{1.5}O_4$ are shown in Fig. 8d. The discharge capacity reduces slightly along with gradually increase of the current density, indicating an outstanding rate performance. As seen in Fig. 8d, with the increasing of current density from 0.2 to 1, 2 and 10 C, the discharge capacities are 143.9, 136.2, 131.9 and 118.6 mAh g^{-1}, respectively. The excellent electrochemical performance of the $LiNi_{0.5}Mn_{1.5}O_4$ might be attributed to its unique core–shell structure with loosely porous configuration and composition of sub-micrometer units, which enlarges the contact area between electrode and electrolyte, shortens the distances for Li^+ migration and decreases the mechanical strain brought by volume swing during the process of Li^+ insertion and extraction.

4. Conclusions

The $LiNi_{0.5}Mn_{1.5}O_4$ with core–shell structure has been successfully synthesized by hydrothermal treatment following a solid-state calcination method. It creates a novel approach to fabricate $LiNi_{0.5}Mn_{1.5}O_4$ microsphere with sub-micrometer units and abundant pores. As-prepared carbonate precursor has a concentration-gradient structure, which might contribute to synthesize core–shell $LiNi_{0.5}Mn_{1.5}O_4$ with excellent cycling performance at elevated temperature and rate capability. The capacity retention can reach to 95% at 55 °C after 30 cycles, and it even delivers a discharge capacity of 118.6 mAh g^{-1} at 10 C at room temperature. Therefore, the $LiNi_{0.5}Mn_{1.5}O_4$ prepared by our route is considered as a promising cathode candidate for lithium-ion batteries to meet requirements of the P-HEV applications.

Acknowledgments

We are grateful for financial support from the Key Research Program of Chinese Academy of Sciences (Grant No. KGZD-EW-202-4), the Natural Science Foundation of Zhejiang (Grant No. LY13B030007), the Key Technology R&D Program of Ningbo (2012B10021), Ningbo Science and Technology Innovation Team (Grant No. 2012B82001).

References

[1] R. Santhanam, B. Rambabu, J. Power Sources 195 (2010) 5442–5451.
[2] J.B. Goodenough, Y. Kim, Chem. Mater. 22 (2010) 587–603.
[3] L. Zhou, D.Y. Zhao, X.W. Lou, Angew. Chem. 123 (2011) 1–4.
[4] J. Wang, X.Y. Yao, X.F. Zhou, Z.P. Liu, J. Mater. Chem. 21 (2011) 2544–2549.
[5] J.G. Li, X.M. He, R.S. Zhao, C.R. Wan, C.Y. Jiang, D.J. Xia, S.C. Zhang, J. Power Sources 158 (2006) 524–528.
[6] Y.G. Liang, X.Y. Han, X.W. Zhou, J.T. Sun, Y.H. Zhou, Electrochem. Commun. 9 (2007) 965–970.
[7] M.H. Zhang, J. Wang, Y.G. Xia, Z.P. Liu, J. Alloys Compd. 518 (2012) 68–73.
[8] J.H. Kim, S.T. Myung, C.S. Yoon, S.G. Kang, Y.K. Sun, Chem. Mater. 16 (2004) 906–914.
[9] M. Aklalouch, J.M. Amarilla, R.M. Rojas, I. Saadoune, J.M. Rojo, Electrochem. Commun. 12 (2010) 548–552.
[10] H.L. Wang, H. xia, M.O. Lai, L. Lu, Electrochem. Commun. 11 (2009) 1539–1542.
[11] Y.K. Fan, J.M. Wang, Z. Tang, W.C. He, J.Q. Zhang, Electrochim. Acta 52 (2007) 3870–3875.
[12] G.B. Zhong, Y.Y. Wang, Y.Q. Yu, C.H. Chen, J. Power Sources 205 (2012) 385–393.
[13] X.L. Xiao, J. Lu, Y.D. Li, Nano Res. 3 (2010) 733–737.
[14] A.S. Arico, P. Bruce, B. Scrosati, J.M. Tarascon, W.V. Schalkwijk, Nat. Mater. 4 (2005) 366–377.
[15] M. Armand, J.M. Tarascon, Nature 451 (2008) 652–657.
[16] Y.K. Sun, K.J. Hong, J. Prakash, K. Amine, Electrochem. Commun. 4 (2002) 344–348.
[17] J. Arrebola, A. Caballero, L. Hernan, J. Morales, E.R. Castellon, J.R.R. Barrado, J. Electrochem. Soc. 154 (2007) A178–A184.
[18] T.Y. Yang, N.Q. Zhang, Y. Lang, K.N. Sun, Electrochim. Acta 56 (2011) 4058–4064.
[19] H.M. Wu, I. Belharouak, A. Abouimrane, Y.K. Sun, K. Amine, J. Power Sources 195 (2010) 2909–2913.
[20] M. Jo, Y.K. Lee, K.M. Kim, J. Cho, J. Electrochem. Soc. 157 (2010) A841–A845.
[21] H. Muroyama, T. Matsui, R. Kikuchi, K. Eguchi, Solid State Ionics 176 (2005) 2467–2470.
[22] A. Kaflak, A. Slosarczyk, W. Kolodziejski, J. Mol. Struct. 997 (2011) 7–14.
[23] S.M. Pourmortazavi, M. Rahimi-Nasrabadi, A.A. Davoudi-Dehaghani, A. Javidan, M.M. Zahedi, S.S. Hajimirsadeghi, Mater. Res. Bull. 47 (2012) 1045–1050.
[24] J.F. Li, S.L. Xiong, X.W. Li, Y.T. Qian, J. Mater. Chem. 22 (2012) 23254–23259.
[25] J.C. Arrebola, A. Caballero, M. Cruz, L. Hernan, J. Morales, E.R. Castellon, Adv. Funct. Mater. 16 (2006) 1904–1912.
[26] L.W. Su, Y. Jing, Z. Zhou, Nanoscale 3 (2011) 3967–3983.
[27] X.L. Wu, S.B. Kim, J. Power Sources 109 (2002) 53–57.
[28] H.S. Fang, Z.X. Wang, B. Zhang, X.H. Li, G.S. Li, Electrochem. Commun. 9 (2007) 1077–1082.